International Journal of Thermal Sciences 78 (2014) 111–123

Contents lists available at ScienceDirect

International Journal of Thermal Sciences

journal homepage: www.elsevier.com/locate/ijts

Optimized multi-floor throughflow micro heat exchangers

Abas Abdoli, George S. Dulikravich*

Florida International University, Department of Mechanical and Materials Engineering, MAIDROC Laboratory, Miami, FL 33174, USA

ARTICLE INFO

Article history:
Received 15 September 2013
Received in revised form
6 December 2013
Accepted 6 December 2013
Available online

Keywords:
Convection heat transfer
Microchannels
Electronics cooling
High heat flux
Design optimization
Conjugate heat transfer

ABSTRACT

Multi-floor networks of straight-through counterflow liquid cooled microchannels have been investigated by performing conjugate heat transfer in a silicon substrate of size 15 × 15 × 1 mm. Two-floor and three-floor cooling configurations were analyzed with different numbers of microchannels on each floor, different diameters of the channels, and different clustering among the floors. Direction of microchannels on each floor changes by 90° from the previous floor. Direction of flow in each microchannel is opposite of the flow direction in its neighbor channels. Conjugate heat transfer analysis was performed by developing a software package which uses quasi-1D thermo-fluid analysis and a fully 3D steady heat conduction analysis. These two solvers are coupled through their common boundaries representing surfaces of the cooling microchannels. Using quasi-1D solver significantly decreases overall computing time and its results are in good agreement with 3D Navier–Stokes equations solver for these types of application. Multi-objective optimization with modeFRONTIER software was performed using response surface approximations and genetic algorithm. Maximizing total amount of heat removed, minimizing coolant pressure drop, minimizing maximum temperature on the hot surface, and minimizing non-uniformity of temperature on the hot surface were four simultaneous objectives of the optimization. Maximum number of cooling microchannels on each floor, diameter ranges of the microchannels on each floor, and vertical clustering range of the floors were the specified constraints. Pareto-optimal solutions demonstrate that thermal loads of 800 W cm^{-2} can be effectively managed with such multi-floor microchannel cooling networks. Two-floor microchannel configuration was also simulated with 1000 W cm^{-2} uniform thermal load and shown to be feasible.

1. Introduction

Cooling systems for new generation portable, telecommunications and military electronic devices with higher capacity of heat removal, higher efficiency and smaller size is one of the challenges in the heat transfer field. One of the cooling system technologies is the cooling microchannel based compact heat sink. Significantly smaller sizes of the microchannels offer major advantage of this method which allows multichip integration. The main challenges of this method are high pressure drop which require higher pumping power, surface temperature non-uniformity, liquid maldistribution, and coolant leaks [1,2]. Microchannel heat sinks have been investigated both experimentally and numerically [3,4]. Colgan et al. [5] investigated practical implementation of a single phase microchannel flow in silicon substrates to enhance removal of heat load up to 300 W cm^{-2} using water as coolant. Walchli et al. [6] applied oscillating flow method on water cooling system for thin form factor high performance electronics with 180 W cm^{-2} heat flux load.

One of the first vestiges of the application of optimization methods to improve channel geometries was in the design of gas turbine blades. Intensive work was performed to maximize cooling efficiency of channel-based networks by means of optimizing their arrangement. Martin and Dulikravich [7,8] presented a fully automated program for inverse design and optimization of internally cooled turbine blades, which was validated against experimental results from Pratt & Whitney. A few years later, Jelisavcic et al. [9] applied hybrid evolutionary optimization to the same concept of channel network optimization for turbo-machinery applications. Hong et al. [10] presented a great effort to enhance the cooling uniformity of microchannel heat exchangers through the design of fractal tree-like networks, attempting to reduce coolant pumping pressure drop. Subsequently, Gonzales et al. [11] executed relevant work comprising 2D microchannel networks optimization. Genetic algorithms have been used by Wei and Joshi [12] to perform single objective optimization in order to minimize overall thermal resistance. Husain and Kim [13] performed single objective optimization

* Corresponding author.
E-mail addresses: aabdo004@fiu.edu (A. Abdoli), dulikrav@fiu.edu (G. S. Dulikravich).

1290-0729/$ – see front matter © 2013 Elsevier Masson SAS. All rights reserved.
http://dx.doi.org/10.1016/j.ijthermalsci.2013.12.008

Nomenclature

A	cross-sectional area of a microchannel
C_f	coefficient of wall friction
C	specific heat per unit mass
CV	coefficient of variation
D_h	hydraulic diameter
f	Darcy friction factor
h	convection heat transfer coefficient
k	thermal conductivity of the fluid
$K = K_{in} + K_{out}$	coefficient of inlet + exit losses
L	microchannel length
$\dot{m}$	mass flow rate
N_u	Nusselt number
P_{er}	perimeter of the microchannel
p	static pressure
P_r	Prandtl number
Q	total heat transferred into fluid
R_e	Reynolds number
S	surface area of the microchannel
T	absolute temperature
T_{ave}	average temperature
V	velocity vector magnitude

Greek symbols

η	efficiency of microchannel cooling
ε	channel inner wall surface roughness
τ_w	wall shear stress
ρ	coolant fluid density
σ	standard deviation

Subscripts

IN	microchannel inlet
OUT	microchannel exit/outlet
W	microchannel wall

using response surface approximation in order to find optimal microchannel width, depth, and fin width. Abdoli and Dulikravich [14] performed multiobjective optimization for 4-floor branching microchannel configurations with 67 design variables in order to improve heat removal and decrease temperature non-uniformity and coolant pumping pressure drop. There is still a need for more research on single-phase flow microchannels in order to increase heat transfer efficiency and decrease temperature non-uniformity and pressure drop [15].

In this paper, a cooling configuration involving multiple floors of microchannels is introduced. The main advantages of using straight through-flow cooling channels rather than branching cooling channels are: a) lower pumping power requirements, b) lower manufacturing cost, c) better uniformity of hot surface temperature; and higher reliability in case of plugs in any of the microchannels.

This work represents a significant improvement over the effort [14,16] to develop high efficiency compact heat exchangers based on optimally branched networks of microchannels.

2. Mathematical model description

An automatic 3D conjugate heat transfer analysis software package (CHETSOLP) was developed to model conjugate heat transfer phenomena and calculate flow-field and temperature field simultaneously in order to assess any microchannel heat sink topology. The most relevant mathematical formulations comprising the CHETSOLP package [16] are described in this section. The working logic of the package is to guess temperature distributions on the walls of the microchannels, solve for the coolant flow-field inside the microchannels, transfer the resulting heat fluxes on the walls of the microchannels to the 3D heat conduction analysis code, solve for temperature field in the solid part of the heat exchanger, update temperature on the walls of the microchannels, and iteratively repeat this procedure until the wall temperatures of the microchannels (initially guessed) converge. Data transfer at the solid/fluid interfaces is performed by a developed boundary condition transfer module that links the fluid and solid domain solvers. CHETSOLP consist of two parts; random geometry generator and analysis solvers.

In this research, microchannels have been arranged in four floors inside the silicon substrate with dimension of 15 × 15 mm (length and width), as shown in Fig. 1. Thickness of substrate was calculated based on number of floors, diameter of floors and vertical clustering values.

Fig. 1b shows one microchannel floor which has several separate straight microchannels. As this figure shows flow direction in each channel is in opposite direction of flow in its neighbor channels.

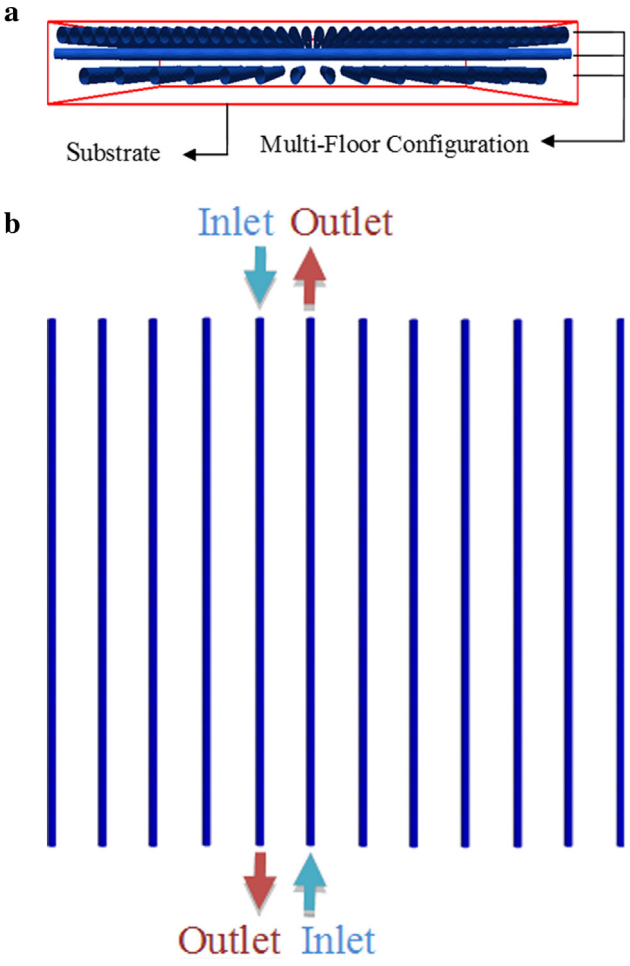

Fig. 1. a) 3D multi-floor microchannels, and b) flow direction in microchannels.

3. Analysis software

In order to perform conjugate heat transfer analysis, two solvers have been coupled to each other; quasi-1D fluid flow and convective heat transfer solver (COOLNET) [7,8] and 3D heat conduction solver (OpenFOAM) [17].

3.1. One-dimensional fluid flow and convective heat transfer analysis (COOLNET)

Each cooling channel was divided in a number of segments (fluid elements). For the lengths and diameters of microchannels considered in this work, numerical experimentation suggested that it is sufficient to divide each channel length in 20 equal length fluid elements.

Balance of momentum equation for such a multifloor network of 1D cooling channel flows involves pressure forces and viscous forces. The viscous forces are typically grouped into major losses forces (due to friction of fluid and the channel wall) and minor losses force (due to flow separation at inlets and exits of each microchannel). Thus, the balance of forces applied to a single, constant hydraulic diameter fluid element in a cooling channel, is typically modeled as

$$0 = p_{\text{in}}A - p_{\text{out}}A - \tau_{\text{w}}S - K\rho\frac{V^2}{2}A \tag{1}$$

Here, A and S represent the cross-section area and wetted surface areas, respectively, of a constant hydraulic diameter fluid element. They are defined in Eq. (3) as functions of the hydraulic diameter, D_{h}, and the perimeter, P_{er}.

$$A = \frac{\pi D_{\text{h}}^2}{4} \quad S = \pi D_{\text{h}}L \quad D_{\text{h}} = \frac{4A}{P_{\text{er}}} \tag{2}$$

The average wall shear stress acting on the fluid inside a channel is approximated in Eq. (3) as a function of the Darcy friction factor and the dynamic pressure.

$$\tau_{\text{w}} = C_{\text{f}}\rho\frac{V^2}{2} = \frac{1}{4}f\rho\frac{V^2}{2} \tag{3}$$

Then, balance of forces in a 1D microchannel is

$$0 = A\left(p_{\text{out}} + \frac{V^2}{2}\right) - A\left(p_{\text{in}} + \frac{V^2}{2}\right) + A\frac{fS}{4A}\rho\frac{V^2}{2} + AK\rho\frac{V^2}{2} \tag{4}$$

This can be rewritten in the matrix form as

$$\begin{bmatrix}\frac{2A}{fV} & -\frac{2A}{fV} & -\frac{1}{4}\frac{S}{A}\end{bmatrix}\begin{Bmatrix}p_{\text{in}} + V^2/2 \\ p_{\text{out}} + V^2/2 \\ A\rho V\end{Bmatrix} = \frac{2A}{fV}\,\text{K}\rho\frac{\text{V}^2}{2} \tag{5}$$

which was used to compute pressure distribution.

Here, Darcy friction factor, f, is calculated for laminar flow conditions as

$$f = \frac{64}{Re} \tag{6}$$

For turbulent flow conditions, it is approximated from Eq. (7) proposed by Chen [18]. Ghanbari et al. [19] demonstrated that Chen's equation is one of the most accurate friction factor equations for straight circular ducts.

$$\frac{1}{\sqrt{f}} = -2\log\left\{\frac{\varepsilon/D_{\text{h}}}{3.7065} - \frac{5.0452}{Re}\log\left[\frac{(\varepsilon/D_{\text{h}})^{1.1098}}{2.8257} + \frac{5.8506}{Re^{0.8981}}\right]\right\} \tag{7}$$

Minor losses in this research are due to inlets and outlets. Loss factors for Eq. (5) were extracted from the data presented by White [20] and Streeter [21] as $K = 0.5$.

Energy balance equation (First Law of Thermodynamics) for quasi-1D steady, incompressible flow results in the extended Bernoulli's equation for the entire channel, in the case of no shaft work, negligible potential energy differences, and no work of electromagnetic forces.

$$\left(\frac{p_{\text{out}}}{\rho} + \frac{V_{\text{out}}^2}{2}\right) = \left(\frac{p_{\text{in}}}{\rho} + \frac{V_{\text{in}}^2}{2}\right) - [(C_{\text{out}}T_{\text{out}}) - (C_{\text{in}}T_{\text{in}})] + \frac{\dot{Q}}{\dot{m}} - \frac{\dot{W}_{\text{visc}}}{\dot{m}} \tag{8}$$

Heat transferred to the fluid by convection is stored in the fluid

$$-[(C_{\text{out}}T_{\text{out}}) - (C_{\text{in}}T_{\text{in}})] + \frac{\dot{Q}}{\dot{m}} = 0 \tag{9}$$

Multiplying Eq. (8) through with $2A\rho/(fV)$ converts it to Eq. (5). If a constant cross-section fluid element is considered, the energy balance of such differential control volume is given by

$$\text{d}\dot{Q} = \dot{m}C\text{d}T = h(T_{\text{w}} - T)\text{d}S \tag{10}$$

which after integration gives the exit fluid bulk temperature that can be computed from Eq. (12), when inlet temperature, wall temperature, heat transfer coefficient, mass flow rate and fluid's specific heat are known.

$$T_{\text{out}} = T_{\text{W}} - (T_{\text{W}} - T_{\text{in}})e^{-hS/\dot{m}C} \tag{11}$$

Then, the rate of heat convected into the flowing fluid can be calculated from

$$\dot{Q} = \dot{m}C(T_{\text{out}} - T_{\text{in}})S \tag{12}$$

The convective heat transfer coefficient, h, can be calculated from Eq. (13) if Nusselt number is known.

$$N_u = \frac{hD_{\text{h}}}{k} \tag{13}$$

To calculate Nusselt number and hence the convective heat transfer coefficient, h, for $0.5 < P_r < 2000$ and $3 \times 10^3 < R_e < 5 \times 10^6$, Gnielinski equation [16], shown as Eq. (14) here, was used. It represents a relationship between the Nusselt, Prandtl and Reynolds numbers and friction factor for steady, incompressible flow in a straight circular cross section tube.

$$N_u = \frac{(f/8)(R_e - 1000)P_r}{1 + 12.7(f/8)^{0.5}\left(P_r^{2/3} - 1\right)} \tag{14}$$

The quasi-1D thermo-fluid solver (COOLNET) is an iterative scheme that decouples continuity and momentum from energy balance. It was formulated, developed and tested by Martin and Dulikravich [7,8,16].

Jelisavcic et al. [9] investigated the COOLNET solver in terms of accuracy and speed against an analytical solution yielded by the Hagen–Poiseuille equation, and also against a high-fidelity 3D Navier–Stokes equations solver (ANSYS CFX). They reported less

than 8% error for the large R_e numbers against analytical solution. They also demonstrated that ANSYS CFX has more accuracy compared to the COOLNET, but at the same time has much higher computational costs. Thus, for research purposes such as the one illustrated in this paper, in which there is a need for simulating many candidate cases, it is highly desirable to use a low cost thermo-fluid analysis such as COOLNET.

The boundary conditions vector stores quantities derived from prescribed values at the domain boundaries. Singular value decomposition algorithm [8] was used for matrix inversion at all iterations. A matrix inversion subroutine solves for equivalent total pressures and mass flow rates simultaneously.

Steady 3D heat conduction analysis inside the heat exchanger solid material was carried out with non-commercial software OpenFOAM [17] which uses the Gaussian finite volume (hexahedral cells) integration method for computation of derivatives and it implements a linear interpolation scheme. A simple advancing-front program (OpenFOAM software [17]) sweeps the micro-channel network solving Laplace's equation for all nodes (except for inlets). The resulting nodal thermal state implies energy balance of the entire network of microchannels.

In another study, Dulikravich and Martin [16] demonstrated the OpenFOAM La Place solver has very high accuracy (error below 1%) against a 2D analytical solution.

Considering the very small sizes of geometries in this study, especially the very small distances between channels, quality of computational grid has the crucial role in the accuracy of 3D heat conduction simulations. It was observed that grids with more than 5,000,000 cells will give the same results in terms of accuracy. In this research the minimum number of hexahedral cells for two-floor configuration was more that 6,000,000 and for three-floor configuration it was more than 7,000,000.

Coefficient of Variation (CV) has been used to study temperature non-uniformity on the hot surface. Coefficient of Variation (CV) was defined as the ratio of standard deviation (σ) over the average value (T_{ave}) of temperature on the hot surface, where N is the number of cells on the surface.

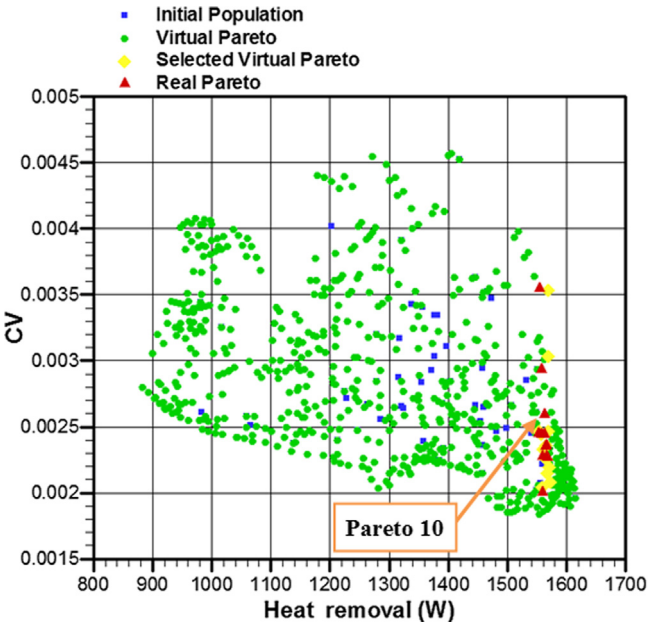

Fig. 3. Two-floor heat removed *vs* CV for initial population, virtual Pareto, and real Pareto optimal designs.

$$\mathrm{CV} = \frac{\sigma}{T_{\mathrm{ave}}} \tag{15}$$

$$\sigma = \sqrt{\frac{1}{N}\sum_{i=1}^{N}(T_i - T_{\mathrm{ave}})^2} \tag{16}$$

$$T_{\mathrm{ave}} = \frac{1}{N}\sum_{i=1}^{N} T_i \tag{17}$$

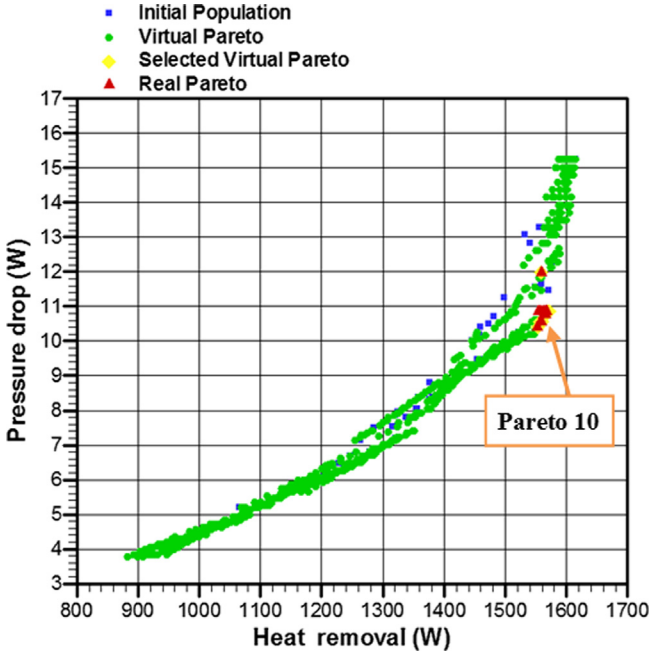

Fig. 2. Two-floor heat removed *vs* coolant pumping power for initial population, virtual Pareto, and real Pareto optimal designs.

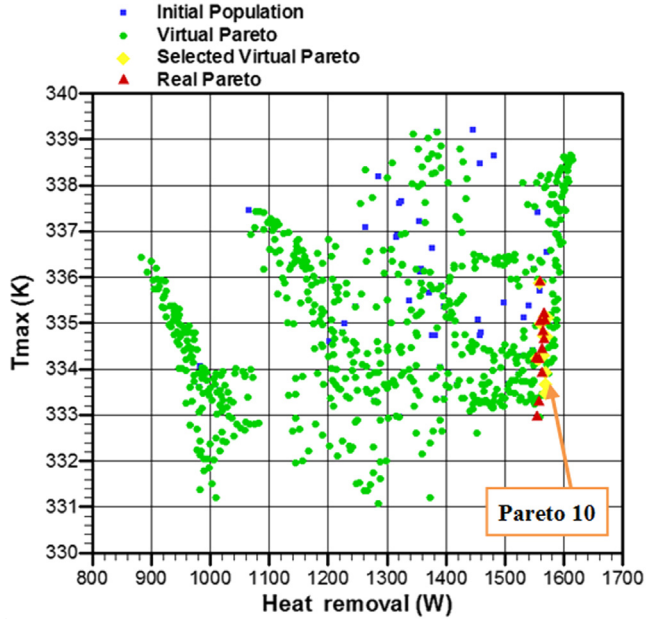

Fig. 4. Two-floor heat removed *vs* T_{max} on hot surface for initial population, virtual Pareto, and real Pareto optimal designs.

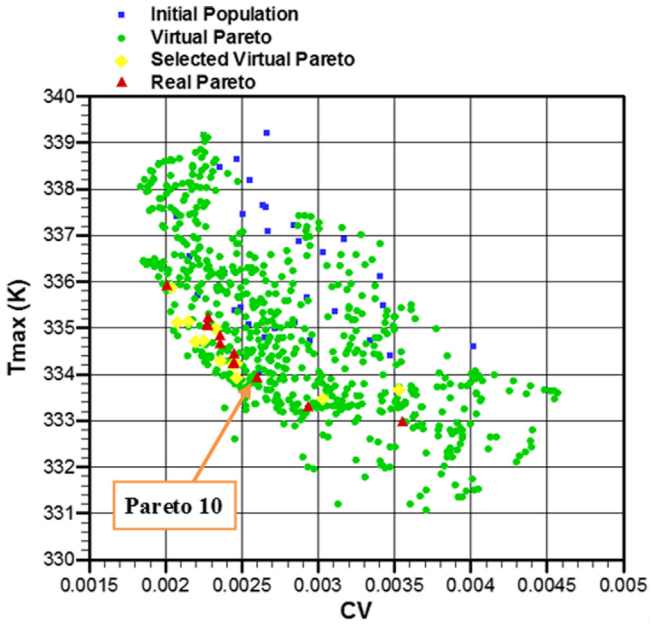

Fig. 5. Two-floor CV *vs* T_{max} on hot surface for initial population, virtual Pareto, and real Pareto optimal designs.

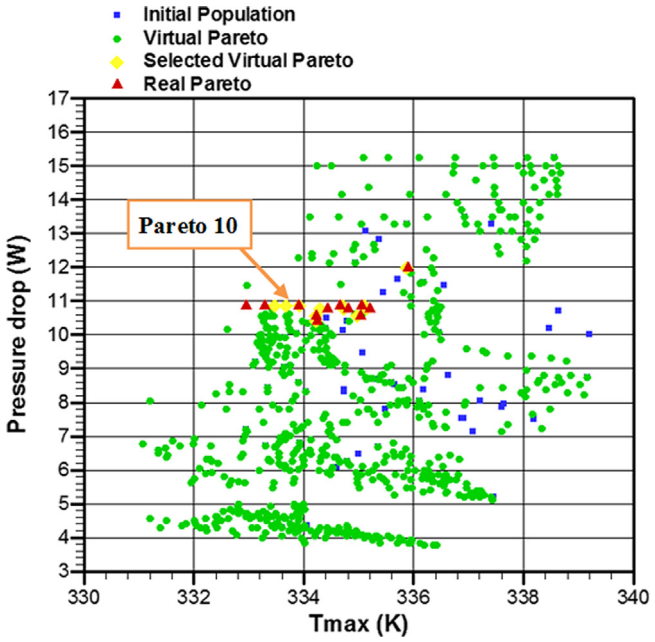

Fig. 7. Two-floor T_{max} on hot surface *vs* pumping power for initial population, virtual Pareto, and real Pareto optimal designs.

4. Multi-objective optimization

Optimization of the topology and geometrical characteristics of the 3D microchannel network was performed by using modeFRONTIER software [22]. In this paper, 2-floor and 3-floor arrangements of microchannels were optimized. Number of straight channels, diameters of the channels on each floor and vertical clustering of floors were design variables in this study. Therefore, the total number of design variables for 2-floor configuration is 5 and for 3-floor configuration is 7. These design variables are randomly varied to generate unique microchannel topologies. Then, these unique random cases were imported to modeFRONTIER to generate multi-dimensional response surfaces (5 dimensional in 2-floor case and 7 dimensional in 3-floor case) to interpolate multivariate scattered data and decrease the computing time significantly. Response Surface Methodology (RSM) was implemented using Gaussian Radial Basis Function (GRBF).

Multi-objective Genetic Algorithm II (NSGA-II) developed by Deb et al. [23,24], was chosen to perform optimization. The four simultaneous objectives of the optimization study were:

1) Maximize total heat removed,
2) Minimize total pressure drop,
3) Minimize temperature non-uniformity on hot surface

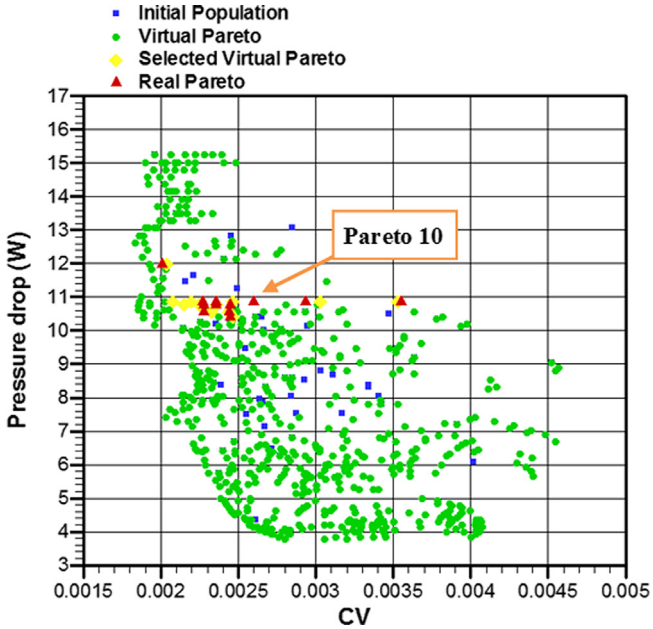

Fig. 6. Two-floor CV *vs* coolant pumping power for initial population, virtual Pareto, and real Pareto optimal designs.

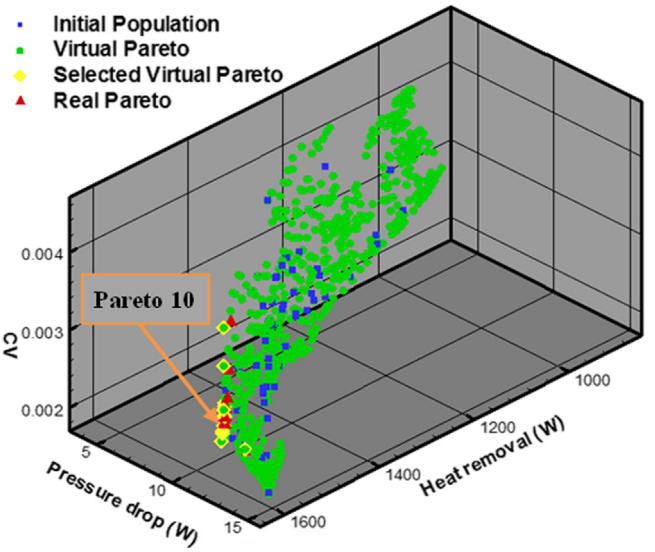

Fig. 8. Two-floor heat removed *vs* pumping power *vs* CV for initial population, virtual Pareto, and real Pareto optimal designs.

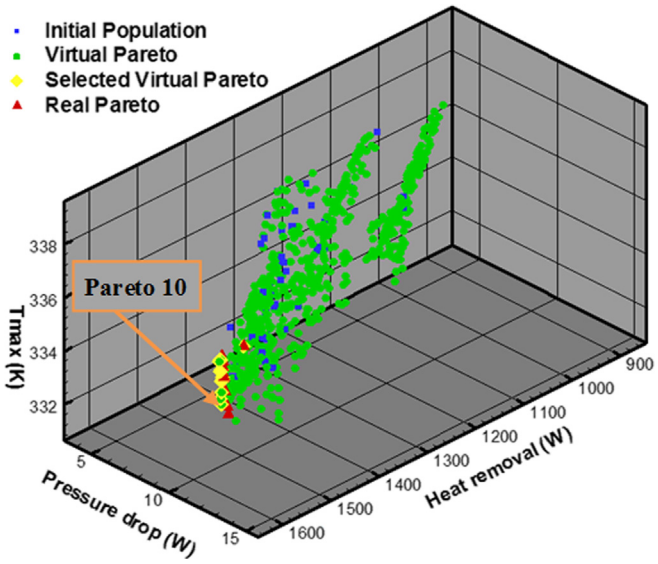

Fig. 9. Two-floor heat removed *vs* pumping power *vs* T_{max} for initial population, virtual Pareto, and real Pareto optimal designs.

Table 1
Two-floor specifications for Pareto design #10.

Floor no.	Number of channels	Microchannel diameter (μm)	Vertical clustering	Substrate thickness (mm)
1	30	200	0.5	0.9
2	40	300		

4) Minimize temperature on hot surface

Constraints in this multi-objective optimization were:

- Number of microchannels on each floor as follows:
  3-floor configuration: 1st floor (10–20), 2nd floor (20–30) and 3rd floor (30–40)
  2-floor configuration: 1st floor (20–30) and 2nd floor (30–40)
- Diameters of microchannels on each floor (200–300 μm)
- Vertical clustering of the floors.

Abdoli and Dulikravich [14] demonstrated that Gaussian Radial Basis Function (GRBF) method gives more accurate results in comparison to other response surface methods. Then, this GRBF was coupled to NSGA-II multi-objective optimization algorithm in modeFRONTIER software in order to perform the optimization.

5. Test case definition

For the purpose of demonstrating the utility of the developed design optimization algorithm for multi-floor networks of cooling channels, we simulated a silicon substrate that has a footprint of 15 mm by 15 mm. Thickness of substrates was calculated based on the number of floors, diameter of channels on each floor and vertical clustering. Thermal conductivity of silicon is 130 W m^{-1} K^{-1}. A uniform thermal load of 800 W cm^{-2} was enforced on the top surface of the substrate and a constant temperature of 300 K was enforced on the bottom surface of the substrate. Water was simulated as pumped at horizontal floors each containing many parallel throughflow microchannels (Fig. 1) to absorb as much heat as possible. Manufacturing limitations [25] constrain microchannel hydraulic diameters to be greater than 100 microns and relative wall roughness was set as 7% of the hydraulic diameter. Diameters of the cooling microchannels were allowed to vary between 200 μm and 300 μm during optimization.

Different investigators have reported different critical Reynolds numbers for fluid flows inside microchannels [26]. In most research, laminar flows were observed for Reynolds number less than 2000. Therefore, in this research, critical Reynolds number has been set at 2000.

The boundary conditions for water coolant at the inlet were: total pressure of 350 kPa and total temperature of 293 K. The boundary condition at the exits was the static pressure of 110 kPa. Fluid properties are temperature-dependent and were imported from OpenFOAM's fluid database [17]. The local average coolant velocities, pressures and temperatures were then calculated by iteratively satisfying a system of local mass conservations and extended Bernoulli's equations [1,3,5].

5.1. Two floor configuration

In two-floor arrangement, the maximum and minimum numbers of microchannels on the first floor were 30 and 20, respectively. For the second floor (close to the hot top surface of the substrate) the maximum and minimum numbers of microchannels were 40 and 30, respectively. An initial population of 79 unique random two-floor configurations of microchannels was generated and simulated using CHETSOLP. Results for one of these optimized cases are shown in this section. Fig. 2 shows the heat removed versus pressure drop for the 79 initial cases represented as blue (in the web version) squares. They were then used to generate multi-dimensional response surfaces using

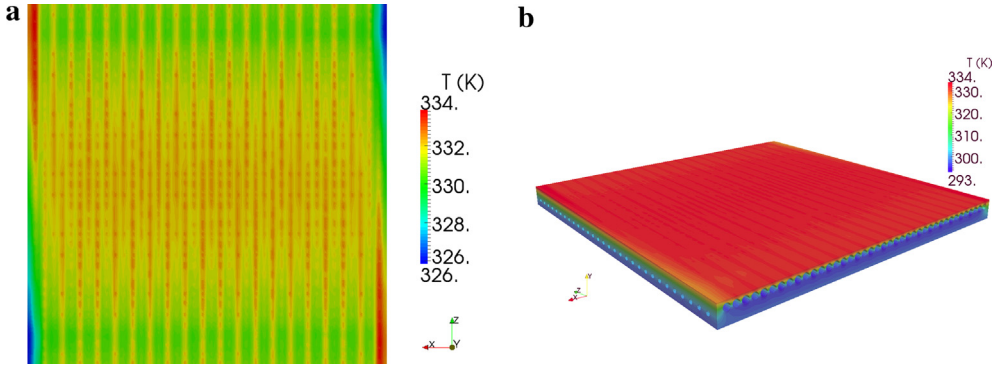

Fig. 10. Two-floor temperature distribution for Pareto optimized design #10 (obtained for 800 W cm^{-2} thermal load): a) hot top surface, and b) entire 3D substrate.

modeFRONTIER software. Multi-objective optimization searches were then performed on these response surfaces. The resulting virtual Pareto front obtained from optimization is illustrated by green circles. Fifteen of these virtual Pareto designs were then chosen (shown as yellow diamonds) as input for 3D conjugate heat transfer analysis software (CHETSOLP) in order to confirm the reliability and accuracy of the response surfaces generated. The analysis results are shown as red triangles and named "Real Pareto". As this figure shows, the real Pareto designs and virtual Pareto designs matched well. One of the best real Pareto designs, Pareto #10, was chosen to be studied in more detail by using its analysis results. Heat removal versus CV has been shown in Fig. 3. Fig. 4 shows heat removal variations versus maximum temperature on the hot surface (T_{max}). Like in Fig. 3, virtual Pareto and initial population were scattered within a discourteous domain. Reason for this is variation of number of microchannels in each floor, especially on the first floor which leads to discontinuity in this domain. This discontinuity can be also observed in Fig. 2. However, since the variation of pressure drop by changing the number of microchannels is less than variation of T_{max} by changing the number of microchannels, therefore the discontinuity in Fig. 4 is more than in Fig. 2.

Fig. 5 shows the T_{max} on hot surface versus CV. As shown in this figure, by increasing T_{max} on hot surface CV will be decreased.

Pressure drop variations versus CV are demonstrated in Fig. 6. Real Pareto designs results are in good agreement with selected virtual Pareto designs (Fig. 7).

More discontinuity is observed in domain of coolant pumping power requirement and T_{max} on hot surface. Pareto #10 was chosen as one of the best optimized designs.

For better illustration, initial population and Pareto designs are shown in a 3D graph Figs. 8 and 9.

Table 1 illustrates the specifications of Pareto design #10. First floor is the closest floor to the cold surface. The data in this table show that Pareto #10 has the maximum number of microchannels and maximum diameters in each floor.

Temperature distributions in Pareto design #10 are shown in Figs. 10 and 11. Fig. 10a and b demonstrates the temperature distribution on the hot surface and the entire substrate, respectively. Temperature on the hot surface is changing from 326 K to 334 K. The CV on the hot surface for this case is 2.598E-03.

Fig. 11a shows temperature distribution on optimized 2-floor microchannels within the substrate. Temperature distributions on the first and second floors are shown in Fig. 11b and c, respectively. Changing the flow direction in each channel will help to improve temperature uniformity.

Table 2 illustrates the mass flow rate, heat removed and pressure drop for each floor. Second floor with 40 channels, which is the closest floor to the hot surface, has the maximum amount of heat removal, mass flow rate and pressure drop.

5.2. Three-floor configuration

For 3-floor arrangement, 146 unique random cases were generated and simulated using CHETSOLP. The maximum and minimum numbers of microchannels in the first floor are 20 and 10, respectively. For the second floor the maximum and minimum numbers of microchannels are 30 and 20, and for the third 40 and 30. Fig. 12 shows the heat removal versus pressure drop for these 146 initial cases in blue (in the web version) squares. The virtual Pareto front obtained from optimization is illustrated by green circles. For validating the optimization results, 15 of these virtual Pareto designs were chosen (shown in yellow diamonds) as input data for 3D conjugate heat transfer analysis software (CHETSOLP). The analysis results of these 15 cases are shown by red triangles and named "Real Pareto". As this figure demonstrates, the real Pareto designs and virtual Pareto designs are in good agreement. For further investigation, one of the best real Pareto designs (Pareto #5) was chosen.

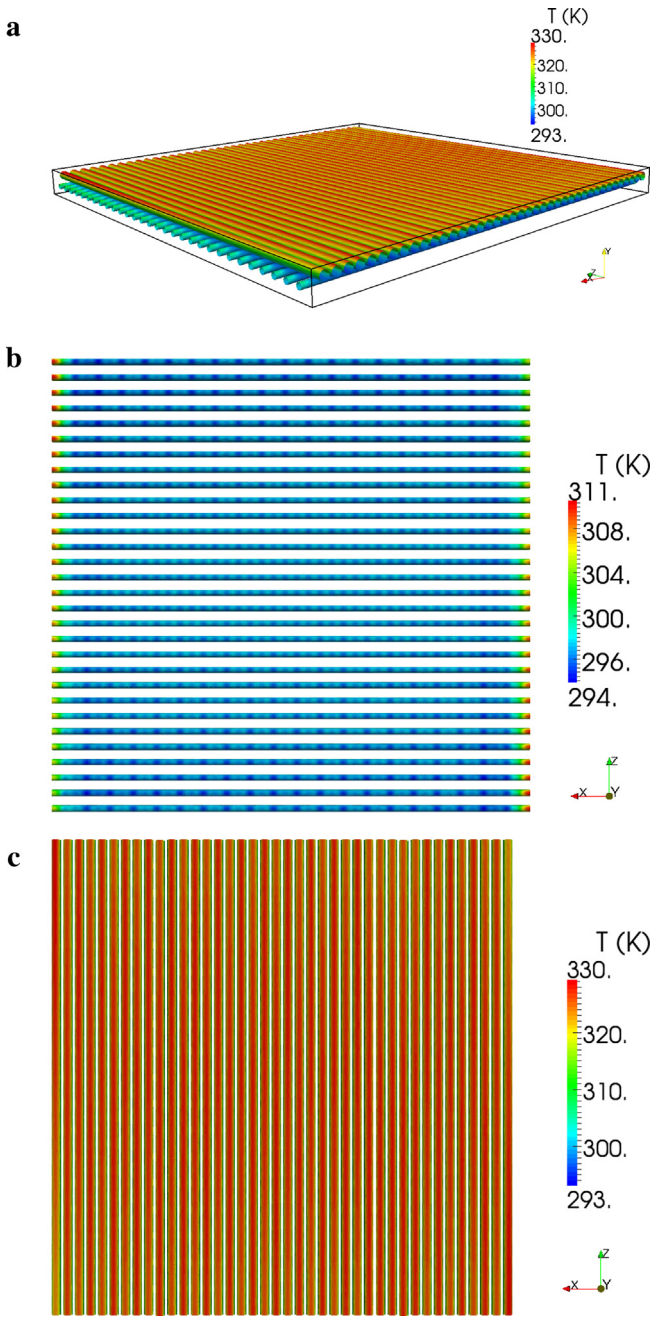

Fig. 11. Two-floor temperature distribution for Pareto optimized design #10 (obtained for 800 W cm^{-2} thermal load): a) microchannels on both floors, b) on 1st floor, c) on 2nd floor.

Table 2
Two-floor results for each floor in Pareto design #10.

Floor no.	Coolant mass flow rate (g/s)	Heat removed (W)	Pumping power requirement (W)
1	8.820	113.933	2.140
2	35.920	1448.409	8.708
Total	44.740	1562.342	10.84732

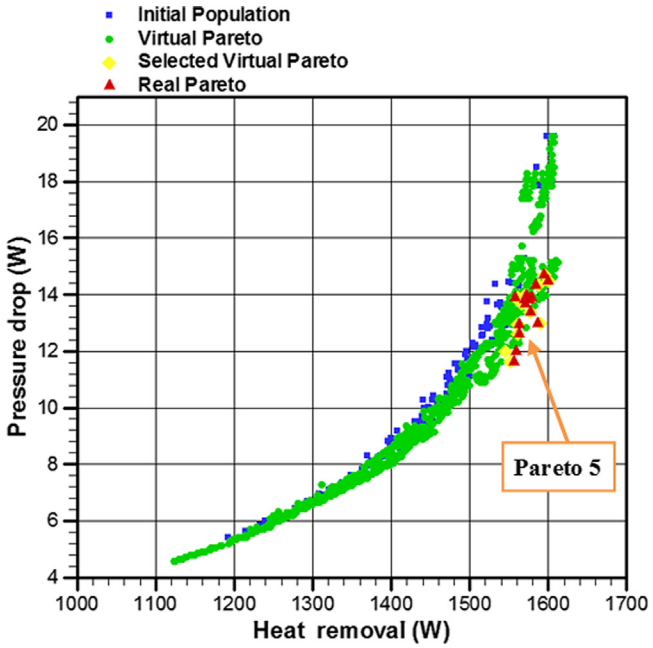

Fig. 12. Three-floor heat removed *vs* pumping power for initial population, virtual Pareto, and real Pareto optimal designs.

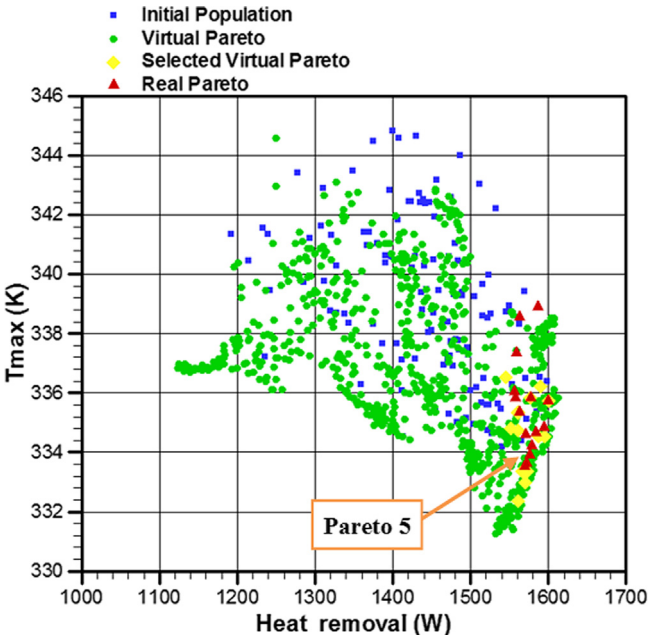

Fig. 14. Three-floor heat removed *vs* T_{max} on hot surface for initial population, virtual Pareto, and real Pareto optimal designs.

Fig. 13 illustrates heat removal variations versus CV. As this figure shows virtual Pareto designs exhibit the same behavior like two-floor arrangement. Real Pareto and selected virtual Pareto designs are in acceptable agreement. Pareto #5 is not the best design in terms of CV, but its T_{max} on hot surface is among the lowest. Having a couple of degrees lower T_{max} on hot surface was considered more important than having the minimum CV. Therefore, Pareto design #5 was chosen to be studied more as our favorite design.

Fig. 15 illustrates the variations of two objectives; CV versus T_{max}. As this figure shows only a few of the design variables are in good agreement with selected virtual Pareto designs. This is because of CV behavior which makes it very hard for response surface to interpolate it accurately.

Heat removal variations versus maximum temperature on hot surface (T_{max}) are shown in Fig. 14. This figure illustrates that Pareto #5 is one of the best designs in terms of lower T_{max} on the hot surface.

Pressure drop variations *vs* CV are shown in Fig. 16. Real Pareto designs are in acceptable agreement with selected virtual Pareto designs.

Variations of pumping power versus T_{max} were demonstrated in Fig. 17.

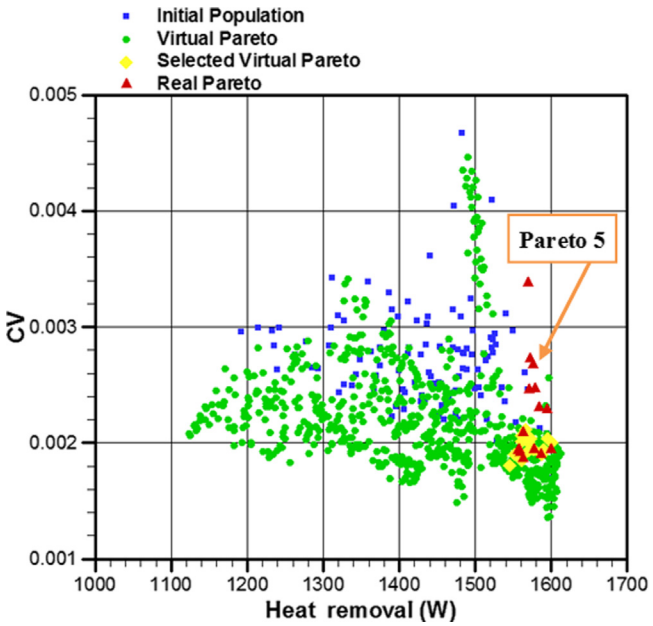

Fig. 13. Three-floor heat removed *vs* CV for initial population, virtual Pareto, and real Pareto optimal designs.

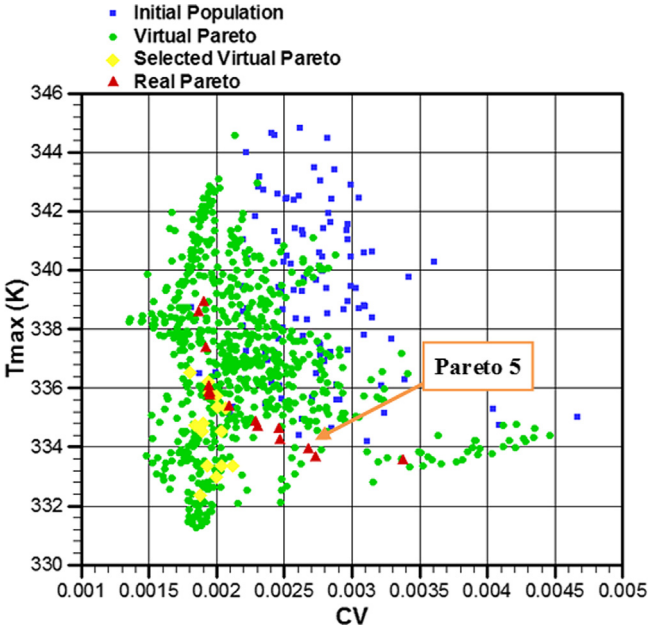

Fig. 15. Three-floor T_{max} *vs* CV on hot surface for initial population, virtual Pareto, and real Pareto optimal designs.

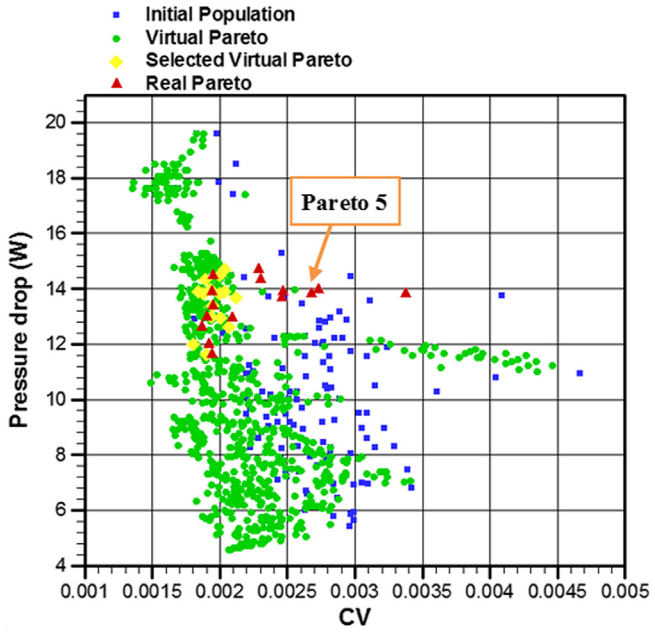

Fig. 16. Three-floor pumping power *vs* CV for initial population, virtual Pareto, and real Pareto optimal designs.

For better illustration, heat removal versus pressure drop versus CV is shown in Fig. 18.

Fig. 19 illustrates the variations of heat removal versus coolant pumping power requirement versus T_{max}.

Specifications of Pareto design #5 is demonstrated in Table 3. First floor is the closest floor to the cold surface. As this table shows Pareto #5 has the maximum number of channels in the third floor (closest to the hot surface) (Table 4).

Figs. 20 and 21 demonstrate temperature distributions in Pareto design #5. Temperature distributions on the hot surface and substrate are shown in Fig. 20a and b. As this figure shows, the maximum temperature on hot surface is 334 K.

Fig. 21 shows temperature distribution on 3-floor micro-channels. Temperature distributions on the 1st, 2nd and 3rd floors are shown in Fig. 21b, c and d, respectively. It is interesting to notice that temperature distribution on the 3rd floor is almost the same as the temperature distribution on the 2nd floor in 2-floor configuration (Fig. 11c).

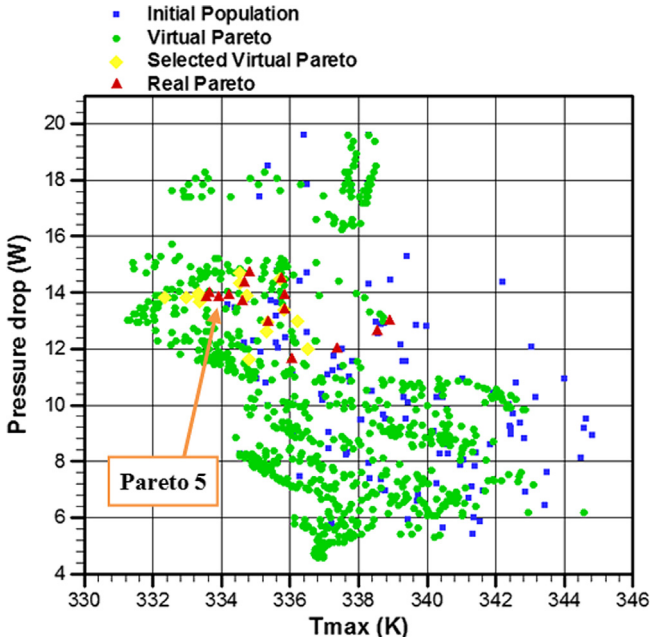

Fig. 17. Three-floor pressure drop *vs* T_{max} on hot surface for initial population, virtual Pareto, and real Pareto optimal designs.

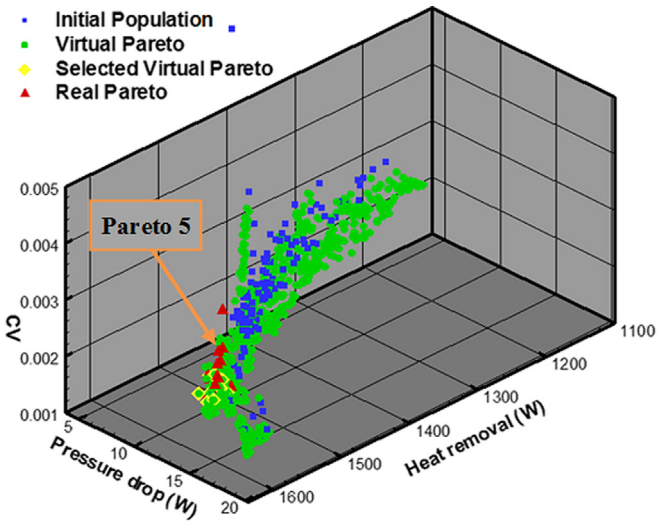

Fig. 18. Three-floor heat removal *vs* pumping power *vs* CV for initial population, virtual Pareto, and real Pareto optimal designs.

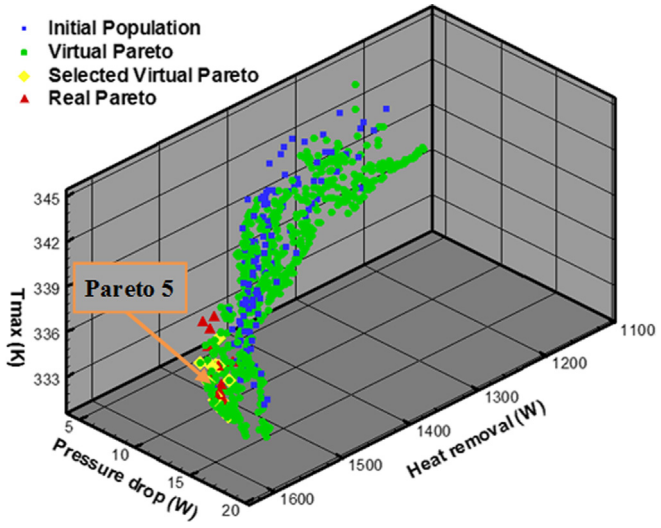

Fig. 19. Three-floor heat removal *vs* pumping power *vs* T_{max} for initial population, virtual Pareto, and real Pareto optimal designs.

Table 3
Specification of 3-floor configuration for Pareto design #5.

Floor no.	Number of channels	Microchannel diameter (μm)	Vertical clustering	Total substrate thickness (mm)
1	14	300	0.8	1.44
2	29	200		
3	40	300		

Table 4
Three-floor analysis results for floors in Pareto design #5.

Floor no.	Mass flow rate (g/s)	Heat removed (W)	Pumping power requirement (W)
1	12.572	116.343	3.048
2	8.526	61.681	2.068
3	35.920	1397.865	8.708
Total	57.018	1575.888	13.824

5.3. Thermal efficiency

Thermal efficiency of microchannel cooling can be studied using the ratio of total heat removed divided by the pumping pressure drop, plus total heat load on the hot surface:

$$\eta = \frac{\text{Power}_{\text{out}}}{\text{Power}_{\text{in}}}\% = \frac{\text{Total heat removed}}{(\text{Total pressure loss} + \text{Heat load})}\% \quad (18)$$

Table 5 shows η and CV for the Pareto optimized case #10 from 2-floor configuration and Pareto optimized case #5 from 3-floor configuration.

By comparing the results, it is observed that in terms of overall thermal efficiency Pareto optimized configuration #10 which has two floors gives practically the same results in terms of CV and T_{max} as Pareto #5 which has a three floor configuration. This strongly suggests that adding third floor has negligible effect on increasing the amount of removed heat and decrease of CV and T_{max} on hot surface.

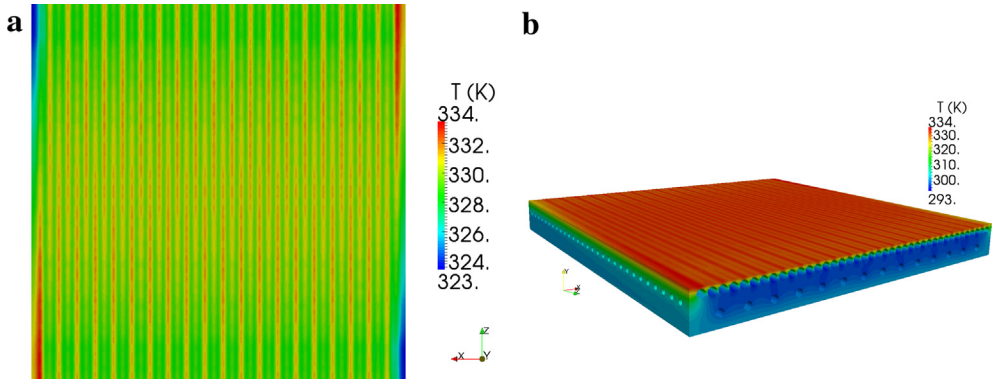

Fig. 20. Three-floor temperature distribution on Pareto design #5 (obtained for 800 W cm^{-2} thermal load): a) hot surface, and b) entire 3D substrate.

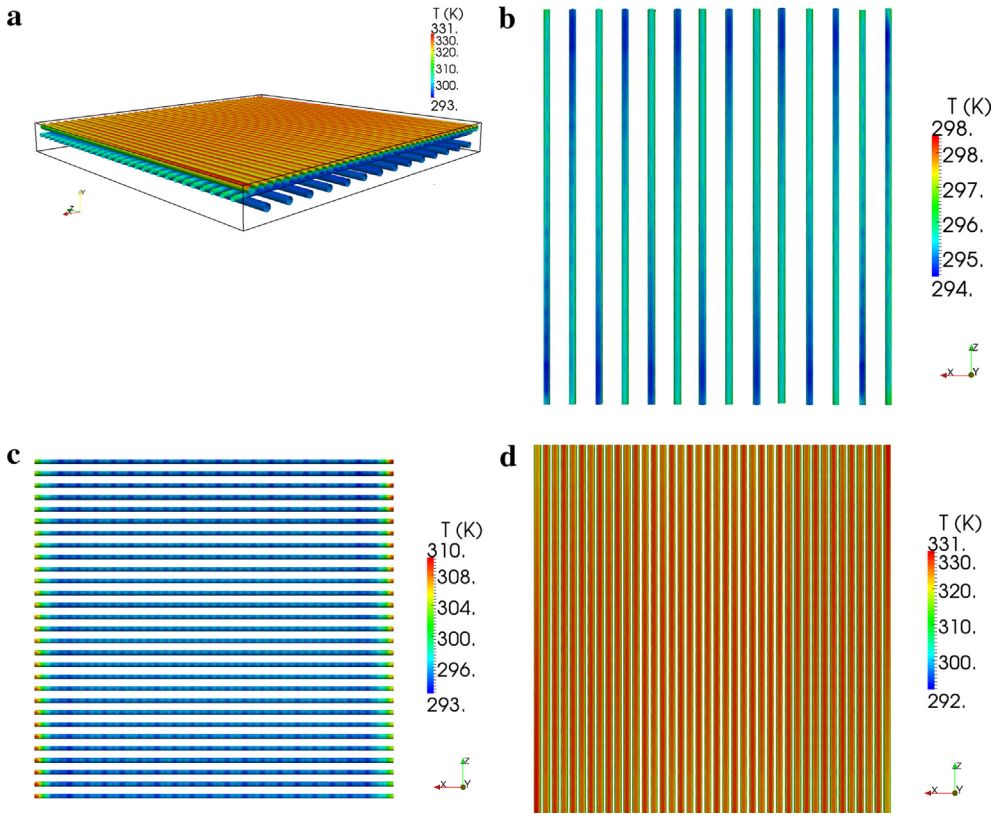

Fig. 21. Three-floor temperature distribution on Pareto design #5 (obtained for 800 W cm^{-2} thermal load): a) 3-floor microchannels, b) 1st floor, c) 2nd floor, and d) 3rd floor.

Table 5
Overall efficiencies and CVs for Pareto optimal 2-floor design# 10 and for Pareto optimal 3-floor design# 5.

Case	η	CV	T_{max} (K)
Pareto #10	86.277	2.598E-03	333.905
Pareto #5	86.882	2.677E-03	333.910

Table 6
Specifications of 2-floor configuration for 1000 W cm^{-2} in case of Pareto design #52.

Floor no.	Number of channels	Floor diameter (μm)	Vertical clustering	Total substrate thickness (mm)
1	38	250	0.5	1
2	40	300		

6. Two floor configuration for 1000 W cm^{-2} heat flux

Therefore, two-floor configuration was chosen as desired configuration for applying a higher heat flux. Specifically, 1000 W cm^{-2} (instead of 800 W cm^{-2}) was applied uniformly on top surface of a silicon substrate. For this case, inlet pressure was 270 kPa which is lower than in the previous test cases. As a result, Reynolds number, thus Nusselt number in cooling channels will decrease. This will create higher hot surface temperature. Other initial and boundary conditions were the same as in Section 5.2. The main objective of this section was to examine the heat removal capacity of the two-floor configuration with 1000 W cm^{-2} heat load. Therefore, one of the best Pareto optimal configuration which had the highest heat removal capacity (Pareto #52) for 800 W cm^{-2} heat load was chosen for simulations with 1000 W cm^{-2} heat load. Table 6 shows the main parameters.

Fig. 22a shows the temperature distribution on the hot surface of the Pareto design #52 having $T_{max} = 358$ K. By using the conjugate heat transfer analysis package (CHETSOLP), the temperature distribution inside the substrate was obtained. Fig. 22b demonstrates temperature distribution on substrate.

Temperature variations on two-floor microchannels are shown in Fig. 23a. As shown in Fig. 23c the maximum temperature on the 2nd floor is 350 K.

Table 7 represents the analysis results of the Pareto design #52 for 1000 W cm^{-2} uniform thermal load demonstrating again that the floor closest to the hot surface has the key role in removing the heat.

From the results shown in Table 8, two-floor configuration has a very high overall thermal efficiency and high T_{max} on hot surface because of increased thermal load.

For better understanding of the overall logic of the software system created, Fig. 24 depicts connections and information flow in the design system used in this paper.

7. Conclusions

In this paper, single phase 3D microchannels with two-floor and three-floor configurations have been investigated using the conjugate heat transfer which combines quasi-1D fluid flow and convective heat transfer solver (COOLNET), and 3D heat conduction solver (OpenFOAM). Each floor consists of a large number of parallel through-flow microchannels.

Multi-objective optimization was performed separately for two-floor and three-floor microchannel configurations. Number of and diameter of microchannels in each floor, and vertical clustering of the floors were design variables for optimization. For two-floor arrangement, total number of design variables was 5 and for 3-floor arrangements it was 7. Maximizing heat removal, minimizing coolant pumping power requirement, temperature non-uniformity and maximum temperature on hot surface were four objectives of this optimization problem. Radial Basis Function (GRBF) for multi-dimensional response surface fitting and interpolation and genetic algorithm (NSGA-II) for evolutionary optimization were chosen to perform the multi-objective optimization task. For 2-floor configuration, 79 random geometries were generated. For 3-floor arrangement, 146 random geometries were generated and analyzed using conjugate heat transfer analysis in order to create GRBF. Fifteen of the virtual Pareto optimal designs obtained from modeFRONTIER were then analyzed using conjugate heat transfer. The simulation results of these 15 designs (real Pareto) have shown good agreement with virtual Pareto optimal designs.

Results of one of the best Pareto designs in each 2-floor and 3-floor configurations were discussed. From results of optimization and by comparing results of Pareto #10 and Pareto #5, the following can be concluded

1. Straight microchannels configurations with opposite flow directions in each channel and 90° shift in floor direction will significantly improve temperature uniformity on hot surface.
2. Last floor (closest floor to the hot surface) has the crucial role in removing the heat.
3. In order to increase heat removal, number and diameter of microchannels on the last floor should be increased.
4. Increasing number of floors does not necessarily increase the amount of heat removed. The 3-floor configuration gives a negligible improvement in overall thermal efficiency.

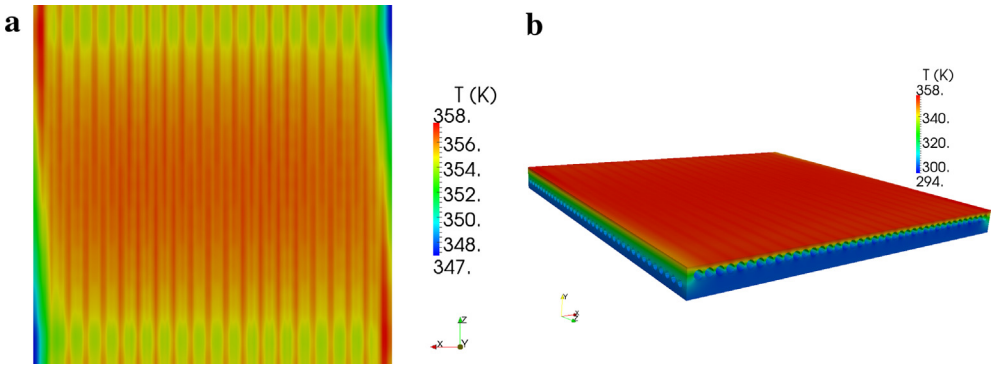

Fig. 22. Temperature distribution on Pareto design #52 (obtained for 800 W cm^{-2} thermal load case) now loaded with 1000 W cm^{-2}: a) hot surface, and b) entire 3D substrate.

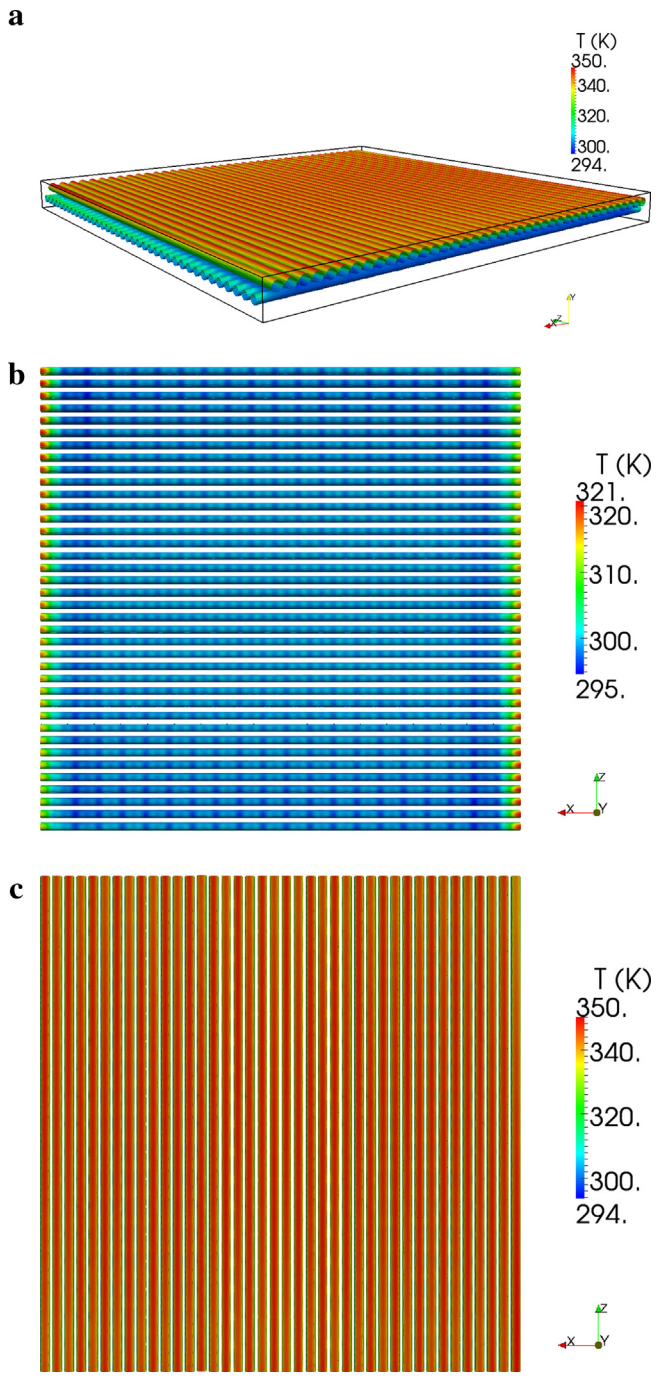

Fig. 23. Temperature distribution for Pareto optimized configuration #52 (obtained for 800 W cm^{-2} thermal load case) now loaded with 1000 W cm^{-2}: a) two-floor microchannels, b) 1st floor, c) 2nd floor.

Table 7
Two-floor analysis results for Pareto optimized design# 52 with 1000 W cm^{-2} uniform heat load.

Floor no.	Mass flow rate (g/s)	Heat removed (W)	Pumping power requirement (W)
1	16.644	244.680	2.693
2	28.96	1863.539	4.681
Total	45.604	2108.219	7.374

Table 8
Overall efficiency, CV and T_{max} for two-floor Pareto optimal design# 52 with 1000 W cm^{-2} uniform heat load.

Case	η	CV	T_{max} (K)
Pareto# 52	93.393	3.283E-03	358.050

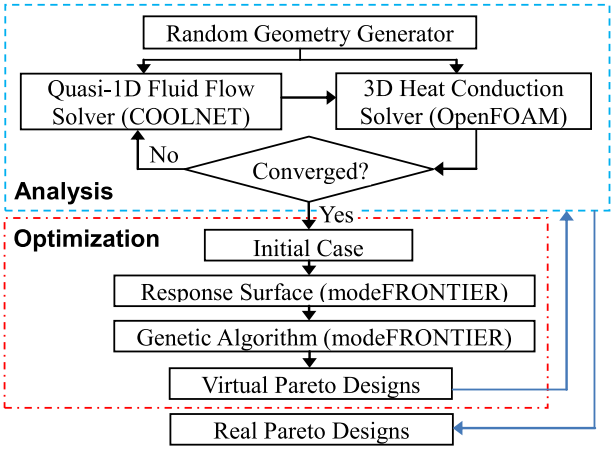

Fig. 24. Flow chart showing how different software modules were linked together to generate virtual and real Pareto frontiers.

In the last section, a two-floor configuration was simulated with 1000 W cm^{-2} uniform heat load. Optimization results show higher thermal efficiency and higher T_{max} with good temperature uniformity on the hot surface.

Acknowledgments

Authors would like to express their gratitude to Prof. Carlo Poloni, founder and president of ESTECO, for providing modeFRONTIER software free of charge for this project.

References

[1] I. Mudawar, Assessment of high-heat-flux thermal management schemes, IEEE Trans. Compon. Packag. Technol. 24 (2001) 122–141.
[2] M.A. Ebadian, C.X. Lin, A review of high-heat-flux heat removal technologies, ASME J. Heat Transfer 133 (11) (2011) 110801.
[3] S.J. Kim, D. Kim, Forced convection cooling in microstructures for electronic equipment cooling, ASME J. Heat Transfer 121 (3) (1999) 639–645.
[4] A.G. Fedorov, R. Viskanta, Three-dimensional conjugate heat transfer in the microchannel heat sink for electronic packaging, Int. J. Heat Mass Transfer 43 (3) (2000) 399–415.
[5] E.G. Colgan, B. Furman, M. Gaynes, W. Graham, N. LaBianca, R.J. Polastre, M.B. Rothwell, Bezama, R. Choudhary, K. Marston, H. Toy, J. Wakil, Zitz, R. Schmidt, A practical implementation of silicon microchannel coolers for high power chips, in: 21st IEEE SEMI-THERM Symposium, 2005, pp. 1–7.
[6] R. Walchli, T. Brunschwiler, B. Michel, D. Poulikakos, Self-contained, oscillating flow liquid cooling system for thin form factor high performance electronics, ASME J. Heat Transfer 132 (5) (2010) 1–9, 051401.
[7] T.J. Martin, G.S. Dulikravich, Aero-thermo-elastic concurrent design optimization of internally cooled turbine blades, in: A.J. Kassab, M.H. Aliabadi (Eds.), Coupled Field Problems, Series on Advances in Boundary Elements, WIT Press, Boston, MA, USA, 2001, pp. 137–184 (Chapter 5).
[8] T.J. Martin, G.S. Dulikravich, Analysis and multi-disciplinary optimization of internal coolant networks in turbine blades, AIAA J. Propuls. Power 18 (4) (2002) 896–906.
[9] N. Jelisavcic, T.J. Martin, R.J. Moral, D. Sahoo, G.S. Dulikravich, M. Gonzalez, Design optimization of networks of cooling passages, Paper IMECE2005–79175, in: ASME IMECE2005, Orlando, Florida, USA, November 5–11, 2005.
[10] F.J. Hong, P. Cheng, H. Ge, T. Joo, Design of a fractal tree-like microchannel net heat sink for microelectronic cooling, 2006. Paper ICNMM2006–96157, ASME Fourth Int. Conf. on Nanochannels, Microchannels and Minichannels, Limerick, Ireland.

[11] M.J. Gonzales, N. Jelisavcic, R.J. Moral, D. Sahoo, G.S. Dulikravich, T.J. Martin, Multi-objective design optimization of topology and performance of branching networks of cooling passages, Int. J. Therm. Sci. 46 (11) (2007) 1191–1202.
[12] X. Wei, Y. Joshi, Optimization study of stacked micro-channel heat sinks for micro-electronic cooling, in: Proceedings of ITherm 2002, San Diego, CA, 2002, pp. 441–448.
[13] A. Husain, K.-Y. Kim, Thermal optimization of a microchannel heat sink with trapezoidal cross section, J. Electron. Packag. 131 (2) (2009) 1–6, 021005.
[14] A. Abdoli, G.S. Dulikravich, Multi-objective design optimization of multi-floor, counterflow micro heat exchangers, Paper HT2013-17738, in: ASME Heat Transfer Conference, Minneapolis, MN, July 14–19, 2013.
[15] S.G. Kandlikar, Microchannels: rapid growth of a nascent technology, ASME J. Heat Transfer 132 (2010) 1–12, 040301.
[16] G.S. Dulikravich, T.J. Martin, Optimization of 3D branching networks of micro-channels for microelectronic device cooling, Paper IHTC14-22719, in: 14th International Heat Transfer Conference – IHTC14, Washington, D.C., August 7–13, 2010.
[17] OpenCFD Ltd, OpenFOAM, 2000, 2013. <http://www.opencfd.co.uk/openfoam/>.
[18] N.-H. Chen, An explicit equation for friction factor in pipe, Ind. Eng. Chem. Fundam. 18 (3) (1979) 296.
[19] A. Ghanbari, F.F. Farshad, H.H. Rieke, Newly developed friction factor correlation for pipe flow and flow assurance, J. Chem. Eng. Mater. Sci. 2 (6) (2011) 83–86.
[20] F.M. White, Fluid Mechanics, sixth ed., McGraw-Hill, New York, 2008.
[21] V.L. Streeter, E.B. Wylie, Fluid Mechanics, eighth ed., McGraw-Hill, New York, 1985.
[22] modeFRONTIER optimization software, <http://www.esteco.com>.
[23] K. Deb, A. Pratap, S. Agarwal, T. Meyarivan, A fast and elitist multi-objective genetic algorithm-NSGA-II, 2000. KanGAL Report Number 2000001.
[24] K. Deb, R.B. Agrawal, Simulated binary crossover for continuous search space, Complex Syst. 9 (1995) 115.
[25] K.W. Jones, Y.-Q. Liu, M.-C. Cao, Micro heat pipes in low temperature cofire ceramic (LTCC) substrates, IEEE Trans. Compon. Packag. Technol. 26 (1) (2003) 110–115.
[26] A.A. Saha, S.K. Mitra, Microfluidics and Nanofluidics Handbook: Chemistry, Physics, and Life Science Principles, Taylor & Francis Group, 2012, pp. 139–155.